PROJECT FINAL REPORT for Korean – AFOSR Nanoscience and Technology Initiative
<AOARD-044049>

< Fabrications and Characterizations of $ZnO/Zn_{1-x}Mg_xO$ Nanorod Quantum Structures >

< November 2, 2005>

Name of Principal Investigator: Prof. Gyu-Chul Yi

Institution: Pohang University of Science and Technology (POSTECH)
Mailing address: National CRI Center for Semiconductor Nanorods
Dept. of Materials Science and Engineering
POSTECH
San-31 Hyoja-dong
Pohang, Gyeongbuk 790-784
Korea (ROK)
Phone: +82-54-279-2155
FAX: +82-54-279-8635
e-mail address: gcyi@postech.ac.kr

Report Documentation Page

Form Approved
OMB No. 0704-0188

1. REPORT DATE	2. REPORT TYPE	3. DATES COVERED
16 FEB 2007	**Final Report (Technical)**	**06-05-2004 to 05-10-2005**

4. TITLE AND SUBTITLE
Fabrications and Characterizations of ZnO/Zn1-xMgxO Nanorod Quantum Structures

5a. CONTRACT NUMBER
5b. GRANT NUMBER
5c. PROGRAM ELEMENT NUMBER

6. AUTHOR(S)
Gyu Chul Yi

5d. PROJECT NUMBER
5e. TASK NUMBER
5f. WORK UNIT NUMBER

7. PERFORMING ORGANIZATION NAME(S) AND ADDRESS(ES)
Pohang Univ. of Science & Technology,San-31 Hyoja-dong,Pohang, Kyungbuk 790-784,Korea ,KE,790-784

8. PERFORMING ORGANIZATION REPORT NUMBER
AOARD-044049

9. SPONSORING/MONITORING AGENCY NAME(S) AND ADDRESS(ES)
The US Resarch Labolatory, AOARD/AFOSR, Unit 45002, APO, AP, 96337-5002

10. SPONSOR/MONITOR'S ACRONYM(S)
AOARD/AFOSR

11. SPONSOR/MONITOR'S REPORT NUMBER(S)

12. DISTRIBUTION/AVAILABILITY STATEMENT
Approved for public release; distribution unlimited

13. SUPPLEMENTARY NOTES

14. ABSTRACT
Recent demonstration of semiconductor nanord heterostructure opens up significant opportunities for fabrication of electronic and photonic nanodevices on single nanords. The semiconductor nanord quantum structures with well defined interfaces are main componens for nanoscale resonant tunneling devises, field effect transistors, and light-emitting devices since the nanord quantum structures (QSs) enable novel physical properties such as quantum confinement to be exploited.

15. SUBJECT TERMS
Nanotechnology, Zinc Oxide

16. SECURITY CLASSIFICATION OF:			17. LIMITATION OF ABSTRACT	18. NUMBER OF PAGES	19a. NAME OF RESPONSIBLE PERSON
a. REPORT	b. ABSTRACT	c. THIS PAGE			
unclassified	**unclassified**	**unclassified**		**11**	

Overview

Recent demonstration of semiconductor nanorod heterostructures opens up significant opportunities for fabrication of electronic and photonic nanodevices on single nanorods. The semiconductor nanorod quantum structures with well-defined interfaces are main components for nanoscale resonant tunneling devices, field effect transistors, and light-emitting devices since the nanorod quantum structures (QSs) enable novel physical properties such as quantum confinement to be exploited. In particular, these nanorod quantum structures enable to tune spectral wavelength by varying the well thickness and enhance the light emission intensity at room temperature, useful for many optical device applications. However, quantum confinement effects in nanowires/nanorod heterostructures have not been easily observed despite recent synthesis of compositionally modulated nanowire superlattices by the vapor–liquid–solid (VLS) growth process. This may result from the relatively broad heterostructure interfaces caused by re-alloying of alternating reactants in the metal catalyst during the condensation-precipitation process. In that case, abrupt interfaces can be obtained using our unique method, a catalyst-free nanorod heteroepitaxial growth technique. This nanorod growth method minimizes the formation of a mixed interfacial layer by utilizing direct adsorption of atoms on the top surface of nanorods. Recently, we demonstrated this to be the case by the fabrication of ZnO/ZnMgO QSs within individual ZnO nanorods. With precise thickness control down to the monolayer level, these heterostructures show the clear signature of quantum confinement, an increasing blue shift with decreasing layer thickness. Nevertheless, optical properties of semiconductor nanorod quantum structures have rarely been reported. In this research, we investigated time-integrated and time-resolved photoluminescent (PL) properties of nanorod QSs including ZnO/ZnMgO nanorod single quantum well structures and ZnO/ZnMgO multishell nanorod quantum structures. In addition, scanning near-field optical microscopy (SNOM) has been used for optical characterizations of individual nanorod QSs.

Introduction

Recent demonstration of semiconductor nanorod heterostructures opens up significant opportunities for fabrication of electronic and photonic nanodevices on single nanorods. Especially, semiconductor nanorod quantum structures with well-defined interfaces are main components for nanoscale resonant tunneling devices, field effect transistors, and light-emitting devices. Recently, we fabricated $ZnO/Zn_{1-x}Mg_xO$ nanorod multiple-quantum-well structures (MQWs) and observed a quantum confinement effect from the nanorod MQWs. Further improvement in fabrication of nanorod heterostructures enables observation of strong room temperature (RT) PL even from nanorod SQWs. Although spectral PL of ZnO MQWs has been examined, a complete understanding of the recombination mechanism of carriers requires both temporal and spectral PL measurements. Time-resolved photoluminescence (TRPL) of nanorod heterostructures can be a powerful technique to investigate exciton dynamics of quantum structures. In this research, we investigated time-integrated and time-resolved photoluminescent (PL) properties of nanorod QSs including ZnO/ZnMgO single-quantum-well nanorod quantum structures.

Meanwhile, optical transmission systems will require nanophotonic integrated circuits composed of nanometer-scale dots to increase data transmission rates and capacity. ZnO nanocrystallite is a promising material for realizing nanophotonic devices at room temperature, due to its large exciton binding energy. Furthermore, recent demonstration of semiconductor nanorod quantum-well structure enables us to fabricate nanometer-scale electronic and photonic devices on single nanorods. Recently, ZnO/ZnMgO nanorod multiple-quantum-well structures (MQWs) were fabricated and the quantum confinement effect was successfully observed. In addition, further improvement in the fabrication of nanorod heterostructures has resulted in the observation of significant PL intensity, even from ZnO/ZnMgO nanorod single-quantum-well structures (SQWs). To confirm the promising optical properties of individual ZnO SQWs for realizing nanphotonic devices, we measured for the first time the photoluminescence (PL) spectra from the isolated ZnO SQWs using a low temperature near-field optical microscope (NOM).

Results

1. Photoluminescent properties of $ZnO/Zn_{0.8}Mg_{0.2}O$ nanorod single-quantum-well structures

During the last research period, we investigated $ZnO/Zn_{0.8}Mg_{0.2}O$ nanorod single-quantum-well (SQW) structures on $Al_2O_3(0001)$ and Si(001) substrates using catalyst-free metal organic vapor phase epitaxy (MOVPE). To fabricate $ZnO/Zn_{0.8}Mg_{0.2}O$ nanorod SQW, high quality ZnO nanorods were grown and $Zn_{0.8}Mg_{0.2}O$ layers were epitaxially grown only on the tips of the ZnO nanorods. For ZnO nanorod synthesis, we used diethylzinc (DEZn) and oxygen as the reactants with argon as the carrier gas. Subsequent $Zn_{0.8}Mg_{0.2}O$ shell layers were deposited by introducing bis-cyclopentadienyl-Mg (Cp_2Mg) as the Mg precursor. A schematic of $ZnO/Zn_{0.8}Mg_{0.2}O$ nanorod SQWs is shown in Figure 1 (a). ZnO well layer thickness (L_w) investigated in this study ranged from 11 to 90 Å while the thicknesses of $Zn_{0.8}Mg_{0.2}O$ bottom and top barrier layers in nanorod SQWs were fixed to 300 and 60 Å, respectively. Electron microscopy images reveal the general morphology of $ZnO/Zn_{0.8}Mg_{0.2}O$ nanorod SQW arrays. As shown in Figure 1 (b), nanorods with a mean diameter of 40 nm were well-aligned vertically over $Al_2O_3(0001)$ substrates.

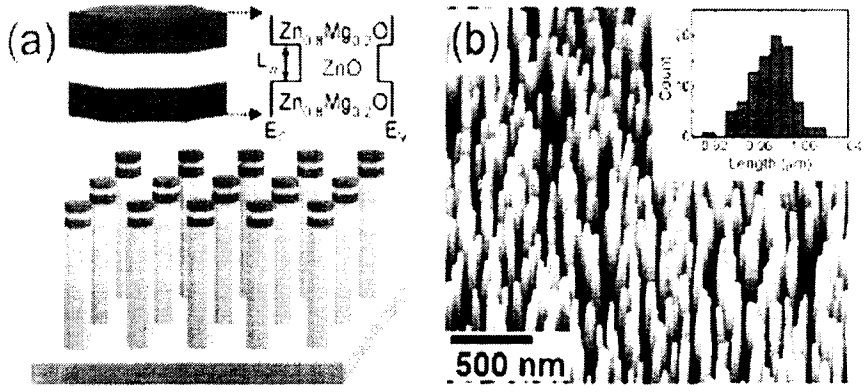

Fig. 1. (a) Schematic illustration of a $ZnO/Zn_{0.8}Mg_{0.2}O$ nanorod SQW structures and SQW electronic band diagram. (b) Tilted view FE-SEM images of nanorod SQWs. The inset of Fig. 1(b) shows the histograms of nanorod length.

Figure 2(a) shows low temperature PL spectra of $ZnO/Zn_{0.8}Mg_{0.2}O$ nanorod heterostructure (with $Zn_{0.8}Mg_{0.2}O$ layer thickness of ~200 nm) and SQWs with different ZnO well layer widths. As shown in Fig. 2, the nanorod heterostructure exhibited only PL peaks at 3.360 eV (I_2^{ZnO}) and 3.58 eV (I^{ZnMgO}) from ZnO nanorod stems and ZnMgO layers, respectively. However, the nanorod SQWs exhibited PL peaks at 3.360–3.366 eV and 3.375–3.518 eV, and the PL peak energy blue-shifted from 10 meV to 160 meV as the well layer width decreased from 90 to 11 Å. Variation in the I_{QW} peak energy depending on the ZnO well layer width as well as theoretical predictions in finite square-well potential are depicted in Fig. 2(b). The experimental data agrees well with the results from theoretical calculations, indicating that the systematic increase in the PL emission peak by reducing the well layer width results from the quantum confinement effect.

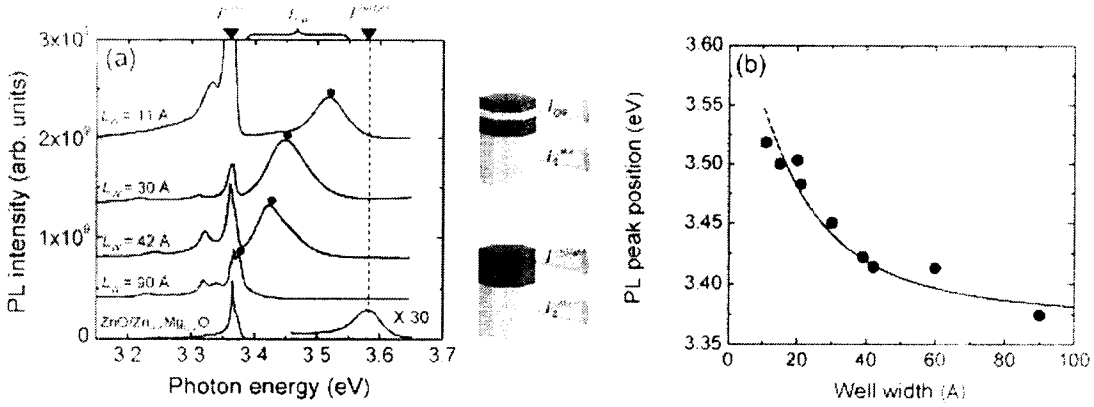

Fig. 2. (a) 10 K PL spectra of ZnO/$Zn_{0.8}Mg_{0.2}O$ nanorod heterostructure and SQWs with different ZnO well layer widths and (b) ZnO well layer width vs. PL peak energy position in ZnO/$Zn_{0.8}Mg_{0.2}O$ nanorod SQWs (closed circles) and theoretically calculated values (dashed curve).

To confirm the origin of the PL peaks, temperature-dependent evolution of the PL peaks in ZnO/$Zn_{0.8}Mg_{0.2}O$ nanorod SQWs was observed. Figure 3 exhibits the typical PL spectra of ZnO/$Zn_{0.8}Mg_{0.2}O$ nanorod SQWs with L_w of 30 Å measured in the temperature range from 10 to 300 K. At 10 K, the strong and sharp peak (I_2) due to bound exciton recombination in ZnO nanorod stems was observed at 3.361 eV, while the broad peak (I_{QW}) with a FWHM of 70 meV appeared at 3.45 eV. The I_{QW} peak originated from the recombination of the excitons at the thin ZnO well layers in the nanorod SQWs. As the temperature increased, the I_2^{ZnO} peak intensity drastically decreased and almost disappeared at temperatures above 90 K, whereas the I_{QW} peak quenched rather slowly and survived even at RT.

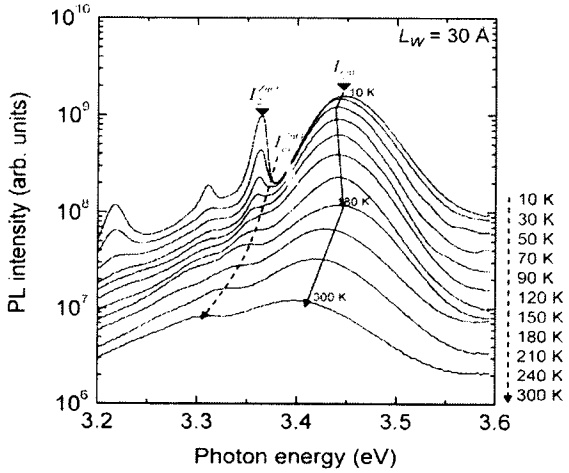

Figure 3. Temperature-dependent PL spectra of ZnO/$Zn_{0.8}Mg_{0.2}O$ SQW nanorods with a well layer width of 30 Å at 10–300 K.

The energy positions of free exciton peak (I_{ex}^{ZnO}) and I_2^{ZnO} decreased with band gap energy shrinkage according to the Varshni's formula as generally observed from ZnO bulk crystals and films. However, the I_{QW} emission peak position exhibits so-called "S-shaped"

behavior, i.e., a red–blue–redshift of the peak position with increasing temperature. As traced by the solid curve in Fig. 3, the I_{QW} peak shows a blueshift of 7 meV in the range of 50–180 K. The blue-shift in the temperature-dependent PL emission is frequently observed from diverse semiconductor thin films with quantum structures, and has been explained in terms of localized states or a piezoelectric field (PEF) effect.

In addition to the TIPL, TRPL of ZnO/$Zn_{0.8}Mg_{0.2}O$ nanorod SQWs were measured in order to investigate exciton dynamics in nanorod SQWs. Figure 4 shows TRPL signals measured at photon energies of 3.36 and 3.43 eV, which correspond to I_2^{ZnO} emitted from ZnO nanorod stems and I_{QW} emitted from thin ZnO single quantum wells in the nanorods, respectively. Both TRPL data of I_2^{ZnO} and I_{QW} fit well with a double exponential decay curve function with a 25–30 ps rise component. The TRPL of I_{QW} shows a slower decay than that of I_2^{ZnO}. From the curve fittings, the decay time constants of I_{QW} are estimated to be 170 and 580 ps, much longer than those of I_2^{ZnO}, 56 and 330 ps. The different PL life times of I_{QW} and I_2^{ZnO} can be explained in terms of size-dependent light-matter interaction in low dimensional nanostructures. Light-matter interaction based on exciton-polariton pictures predicted that radiative recombination time increases as size decreases in cases where particle size is small enough to be comparable to the exciton Bohr diameter. Additionally, the thermal release effect of excitons from localized to delocalized states at the wells might also increase the PL life time.

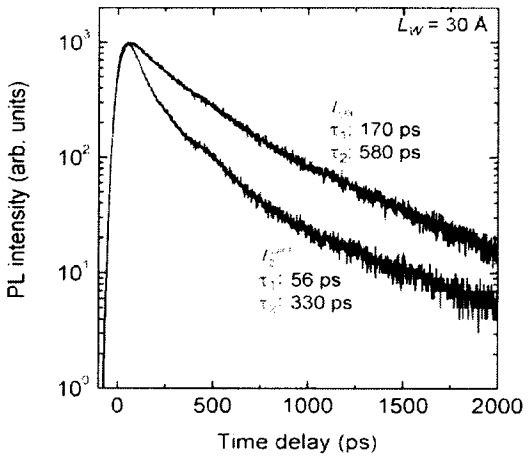

Figure 4. TRPL data of bound exciton (I_2^{ZnO}) emitted from ZnO nanorod stems and I_{QW} emitted from thin ZnO quantum well layers obtained from ZnO/$Zn_{0.8}Mg_{0.2}O$ nanorod SQWs with a well layer width of 30 Å

The results on photoluminescent properties of ZnO/$Zn_{0.8}Mg_{0.2}O$ nanorod SQW structures shown here provide insights for understanding optical properties and exciton dynamics of semiconductor nanorod quantum structures

2. Fabrications and quantum confinement of ZnO/ZnMgO multishell nanorod quantum structures

During the last research period, we fabricated $ZnO/Zn_{0.8}Mg_{0.2}O/ZnO/Zn_{0.8}Mg_{0.2}O$ multishell nanorod heterostructures on $Al_2O_3(0001)$ and Si(001) substrates using catalyst-free metal organic vapor phase epitaxy (MOVPE). For core ZnO nanorod synthesis, we used diethylzinc (DEZn) and oxygen as the reactants with argon as the carrier gas. Subsequent $Zn_{0.8}Mg_{0.2}O$ shell layers were deposited by introducing bis-cyclopentadienyl-Mg (Cp_2Mg) as the Mg precursor. The multishell nanorod heterostructures, as schematically depicted in Figure 5, were prepared by repeated alternate deposition of ZnO and $Zn_{0.8}Mg_{0.2}O$ layers repeatedly. The nanorods with various ZnO quantum well (QW) widths, L_W, were prepared in order to investigate the quantum confinement effect. Such distinctive coaxial nanorod structures were realized by precise control of L_W and L_B in angstrom scale using a computer-controlled gas valve system in our MOVPE system. In particular, the formation of interfacial intermediate alloy layers was prevented by purging the system with pure argon whenever the reactants were delivered into the system, leading to formation of clean and abrupt interfaces.

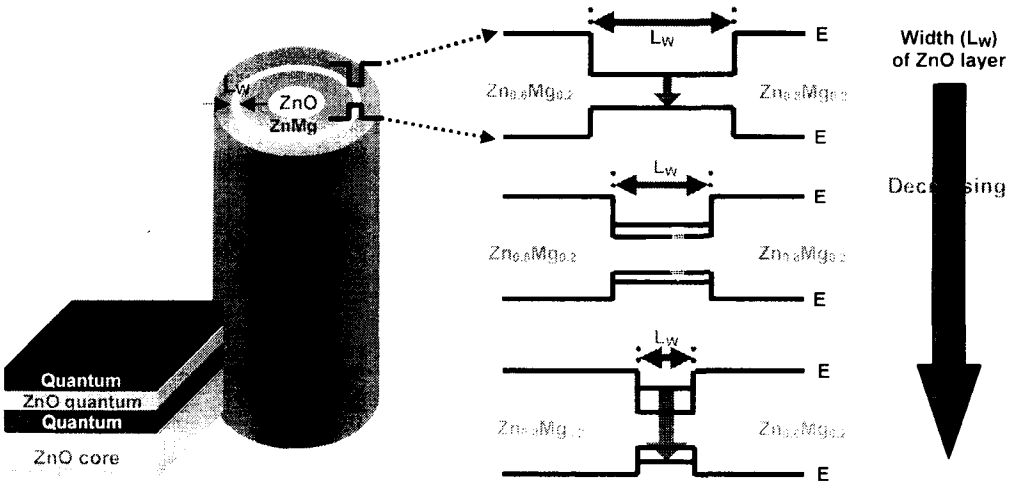

Fig. 5. Schematic illustration of a $ZnO/Zn_{0.8}Mg_{0.2}O/ZnO/Zn_{0.8}Mg_{0.2}O$ multishell nanorod heterostructure and its band diagrams for different ZnO (QW) shell widths (L_W).

The general morphology of the nanorod heterostructures was investigated using field-emission scanning electron microscopy (FE-SEM). As shown in Figure 6(a), the mean diameter and length of bare ZnO nanorods, grown at 800°C for 2 hrs, are 26 nm and 2.5 μm, respectively. Subsequent growth processes of the ZnO (QW) and $Zn_{0.8}Mg_{0.2}O$ (QB) shell layers gradually increased the nanorod diameter: a growth time of QB layer of 30, 60, and 180 sec. produced nanorod heterostructures with various diameters of 51, 52, and 58 nm, respectively. Growth rates of the ZnO (QW) and $Zn_{0.8}Mg_{0.2}O$ (QB) shells were roughly 0.25 and 0.33 Å/sec.

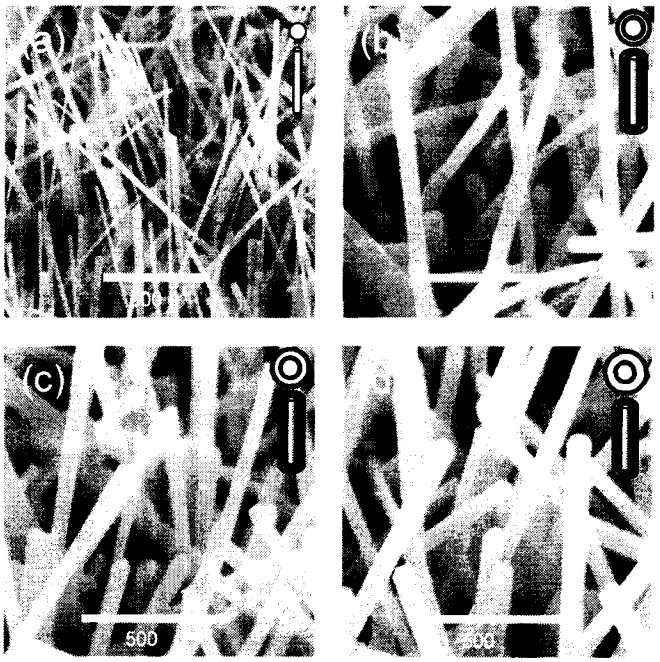

Figure 6. FE-SEM images of (a) bare ZnO nanorods and (b–d) core/multishell nanorod heterostructures. For multishell nanorod heterostructures, ZnO (QW) shell layer growth times were varied as 30, 60, 180 sec, respectively, with a fixed $Zn_{0.8}Mg_{0.2}O$ (QB) shell layer growth time of 180 sec, resulting in their average nanorod diameters of 51, 52, 58 nm.

Figure 7 shows 10 K PL spectra of the $ZnO/Zn_{0.8}Mg_{0.2}O$ core/shell (a) and $ZnO/Zn_{0.8}Mg_{0.2}O/ZnO/Zn_{0.8}Mg_{0.2}O$ multishell (b–e) nanorod heterostructures. The schematic diagrams of the heterostructures are also shown in Fig. 7. PL spectra of the $ZnO/Zn_{0.8}Mg_{0.2}O$ core/shell nanorods exhibited two dominant PL peaks at 3.364 and 3.353 eV corresponding to excitonic emissions from ZnO core nanorods ($I_2^{ZnO\ (core)}$) and $Zn_{0.8}Mg_{0.2}O$ (I^{ZnMgO}) shell layers, respectively. Except for these PL peaks, no PL peak is shown in the range between the 3.364 and 3.353 eV, strongly suggesting that there is no significant intermediate layer formation between ZnO core and $Zn_{0.8}Mg_{0.2}O$ shell layers. If there is an intermediate layer between the ZnO core and $Zn_{0.8}Mg_{0.2}O$ shell layers, there should be at least one additional PL peak between 3.364 and 3.553 eV.

Meanwhile, $ZnO/Zn_{0.8}Mg_{0.2}O/ZnO/Zn_{0.8}Mg_{0.2}O$ core/multishell nanorod heterostructures with various L_W, from 8 to 45 Å, and fixed L_B of 120 Å, showed a new PL peak marked by $I^{ZnO\ (QW)}$. The $I^{ZnO\ (QW)}$ peak energy increases from 3.382 to 3.467 eV, as the L_W is decreased from 45 to 8 Å. All the $I^{ZnO\ (QW)}$ peaks blue-shift toward higher energy, compared with 3.364 eV of $I^{ZnO\ (core)}$. Such a blue-shift of the PL emission peak can be well understood by the fact that quantized sublevel states are created due to the quantum size effect in core/multishell nanorod heterostructures and quantized energy levels increase by decreasing the embedded ZnO (QW) shell layer width, L_W.

Compositional intermixing of ZnO and $Zn_{0.8}Mg_{0.2}O$ at the interface also may cause a blue-shift of the PL peaks. To rule out this possibility, we prepared $ZnO/Zn_{0.8}Mg_{0.2}O/ZnO/Zn_{0.8}Mg_{0.2}O$ multishell nanorods with two different L_W (12 and 78 nm) and fixed L_W (30 Å). Intermixing at the interface may cause a couple of effects: (1) the Mg mole

fraction in the alloy becomes higher by increasing the $Zn_{0.8}Mg_{0.2}O$ shell layer thickness (or growth time), resulting in a larger PL peak blue-shift; (2) effective ZnO (QW) shell thickness can be altered. As shown in Figure 8, the $I^{ZnO(QW)}$ peak positions of the two nanorods are nearly the same, ruling out the intermixing possibility. This clearly indicates that the PL blue-shift in multishell nanorods results from the quantum confinement effect.

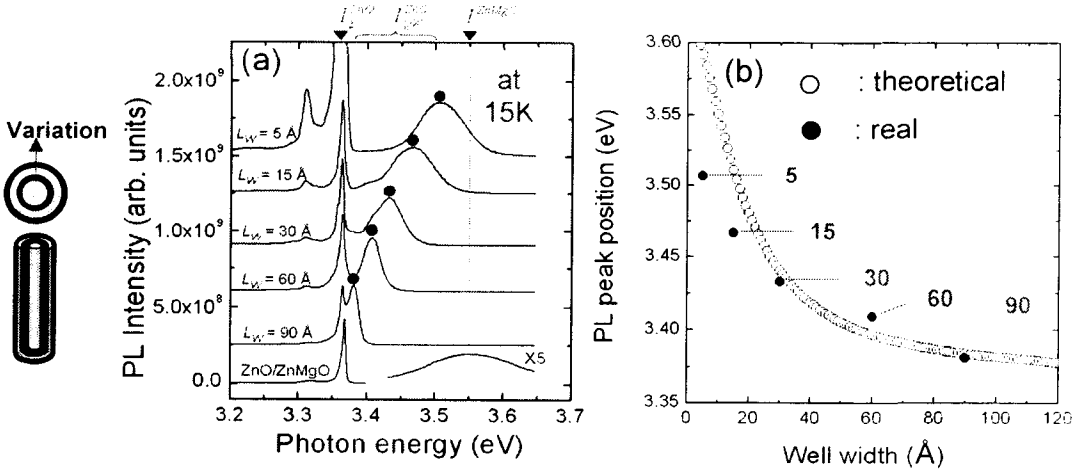

Figure 7. 10 K PL spectra of (a) $ZnO/Zn_{0.8}Mg_{0.2}O$ core/shell nanorod heterostructures and (b–e) $ZnO/Zn_{0.8}Mg_{0.2}O/ZnO/Zn_{0.8}Mg_{0.2}O$ multishell nanorod quantum structures with different ZnO (QW) shell widths of 45, 30, 15, 8 Å.

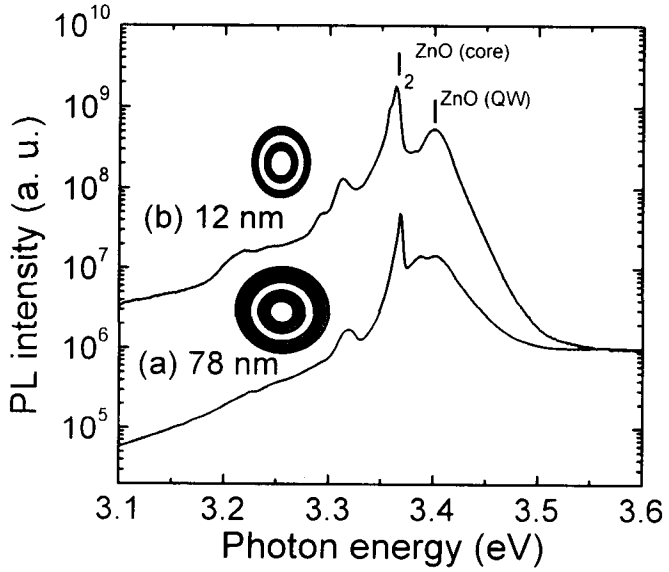

Figure 8. 10 K PL spectra of $ZnO/Zn_{0.8}Mg_{0.2}O/ZnO/Zn_{0.8}Mg_{0.2}O$ multishell nanorods upon variation of different $Zn_{0.8}Mg_{0.2}O$ (QB) shell widths of 12 and 78 nm. The $Zn_{0.8}Mg_{0.2}O$ (QB) shell layer thickness was fixed at 120 Å. Cross-sectional views, ZnO (QW) shell widths, and $Zn_{0.8}Mg_{0.2}O$ (QB) barrier widths of co-axial nanorod heterostructures are depicted in the inset, respectively.

The realization of diverse nanorod QSs offers us the opportunity to observe new physical phenomena in semiconductor nanostructures. Further research will include formation of low dimensional carrier gas, quantized conductance and ballistic transport. This research will open new field on nanorod science and technology.

3. Evaluation of the quantum confinement effect of isolated ZnO nanorod single-quantum-well structures using near-field ultraviolet photoluminescence spectroscopy

ZnO/ZnMgO SQWs were fabricated on the ends of ZnO nanorods with a mean diameter of 40 nm using catalyst-free metalorganic vapor phase epitaxy. The average concentration of Mg in the ZnMgO layers used in this study was determined to be 20 at. %. The ZnO well layer thickness L_w investigated in this study were 2.5, 3.75, and 5.0 nm, while the thickness of the ZnMgO bottom and top barrier layers in the SQWs were fixed at 60 and 18 nm, respectively. After the growth of ZnO nanorod SQWs on sapphire (0001) substrate, they were dispersed on the substrate to be isolated. To confirm the promising optical properties of individual ZnO SQWs, we used collection-mode NOM at 15K, in which He-Cd laser (λ=325 nm) was used for the excitation. We used UV fiber probe with an aperture diameter of 30 nm [Fig. 9].

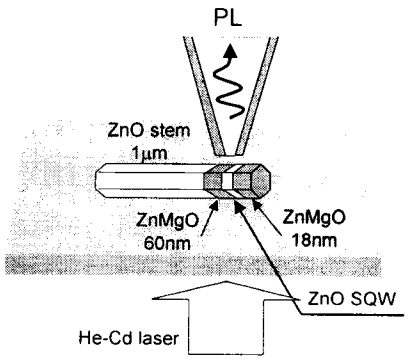

Figure 9. Schematic of near-field spectroscopy of the isolated ZnO SQWs on the ends of ZnO nanorod.

In the near-field spectra, the emission peaks around at 3.365 and 3.52 eV are originated from the neutral-donor bound exciton (D_OX) in the ZnO stem, and the free exciton in ZnMgO layers, respectively, which correspond to that of far-field spectra [dashed curves in Fig. 10(a)]. However, at the well layer, the emission from D_OX was suppressed, while blue-shifted PL emission peak was emerged at 3.499 (L_w = 2.5 nm), 3.444 (L_w = 3.75 nm), and 3.410 eV (L_w = 5.0 nm), respectively. The value of the blue shift was consistent with the theoretical prediction using finite square-well potential of the quantum confinement effect in the ZnO well layer. Spatial distributions of the optical near-field intensity for ZnO SQWs of L_w = 3.75 nm [Figs. 10(b) and (c)] also supported that the blue-shifted emission peaks were confined in the end of the ZnO stem. Furthermore, their spectral width (3 meV) for ZnO SQWs of L_w = 2.5 nm and L_w = 3.75 nm were much narrower than those of far-field spectra (40 meV).

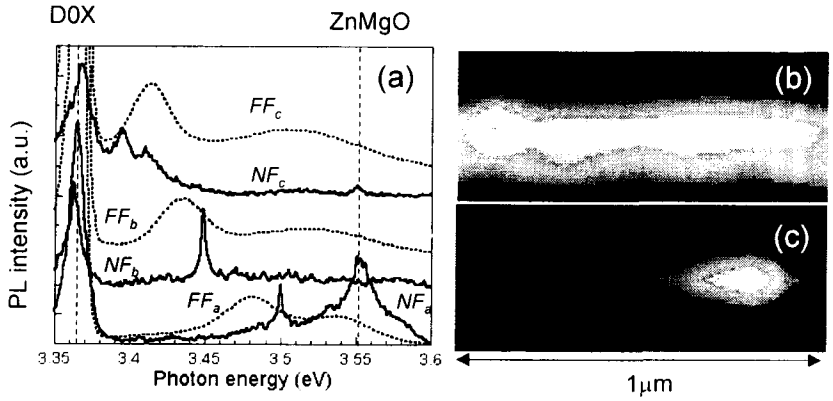

Figure 10. (a) Size-dependent PL spectra of the isolated ZnO nanorod SQWs with L_W = 2.5 nm (FF_a, NF_a), 3.75 nm (FF_b, NF_b), and 5.0 nm (FF_c, NF_c), respectively, obtained at 15 K. FF: far-field spectrum of vertically aligned ZnO nanorod SQWs. NF: near-field PL spectrum of the isolated ZnO SQWs obtained at the well layer. Near-field intensity distributions of the isolated ZnO SQWs (L_W = 3.75 nm) obtained at (b) 3.365 and (c) 3.444 eV, respectively.

In order to estimate the linewidth of the isolated ZnO SQWs, we observed the power-dependent PL spectra of L_W = 3.75 nm [Fig. 11(a)] at various excitation densities ranging from 0.6 to 4.8 W/cm^2. The line shape of each spectrum can be reproduced by the Lorentzian function indicated by the solid line. As shown in Figs. 11(b) and (c), the integrated PL intensity (I_{PL}) linearly increases and the homogeneous width (Δ) is maintained constant around 3 meV. These results indicate that the emission line at 3.444 eV can be identified as emission from a single-exciton state in a ZnO SQWs, and the linewidth of the PL spectra is governed by the homogeneous broadening, which is owing to the internal electric field effect in ZnO or large stem width (40 nm).

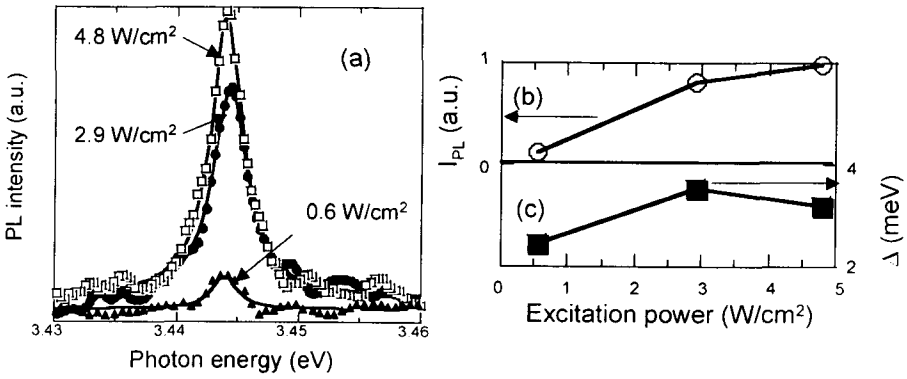

Figure 11. (a) Low-temperature (15 K) near-field PL spectrum of the isolated ZnO SQWs (L_W=3.75 nm) at various excitation densities ranging from 0.6 to 4.8 W/cm^2. Power dependence of (b) the integrated PL intensity I_{PL} and (c) the linewidth (Δ).

The results shown here provide criteria for designing nanophotonic devices, such as the switching devices by controlling the dipole forbidden optical energy transfer among resonant energy states in quantum dots.